Computational Calculation of Dissolved Organic Matter Absorption Spectra

Frank Leresche [#,a,b,*], Elena Vialykh [#,a,b], and Fernando L. Rosario-Ortiz [a,b]

[a] Department of Civil, Environmental, and Architectural Engineering
University of Colorado Boulder, CO 80309

[b] Environmental Engineering Program
University of Colorado Boulder, CO 80309

[#] F.L. and E.V. contributed equally to this paper.

[*]Corresponding author: Frank.Leresche@colorado.edu

KEYWORDS

Absorption, Dissolved Organic Matter, chromophore, DFT calculations, Charge transfer.

SYNOPSIS

The absorption of dissolved organic matter was investigated using computational models. The results indicate that it was possible to approximately recreate DOM spectra by summing individual chromophores spectra.

26 **TOC Art**

27

28

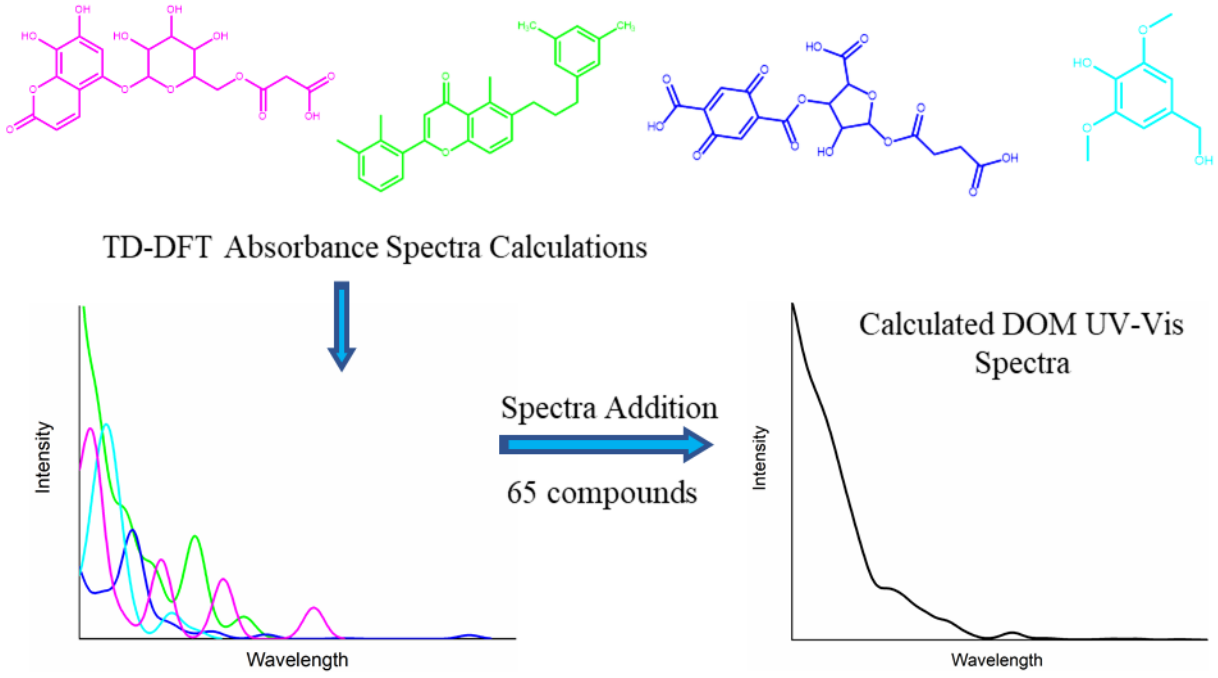

29

ABSTRACT

The absorption spectrum of dissolved organic matter (DOM) is a topic of interest to environmental scientists and engineers, as it can be used to assess both the concentration and physicochemical properties of DOM. In this study, the UV-Vis spectra for DOM model compounds were calculated using time-dependent density functional theory (TD-DFT). Summing these individual spectra, it was possible to recreate the observed exponential shape of the DOM absorption spectra. Additionally, by predicting the effects of sodium borohydride reduction on the model compounds, then calculating the UV-Vis absorbance spectra of the reduced compounds, it was also possible to correctly predict the effects of borohydride reduction on DOM absorbance spectra with a larger relative decrease in absorbance at longer wavelengths. The contribution of charge-transfer (CT) interactions to DOM absorption were also evaluated and the calculations showed that *intra*-molecular CT interactions could take place, while *inter-molecular* CT interactions are proposed to be less likely to contribute.

INTRODUCTION

The absorption spectrum of dissolved organic matter (DOM) is one of its most studied properties. In the early stages of DOM research, absorption spectra were used as a proxy for the concentration of DOM in surface waters.[1] Over the past decades, the use of the absorption spectra has evolved from a quantitative surrogate for concentration, to a qualitative descriptor for physicochemical reactivity and biogeochemical origin. For example, the specific UV absorption at 254 nm ($SUVA_{254}$) has become one of the most widely used optical parameters to describe DOM physicochemical reactivity and character, in settings from assessment of DOM reactivity during drinking water treatment all the way to biogeochemical source. [2-5] In addition, a wide range of metrics derived from the absorption spectra have been developed and implemented by the environmental science and engineering community, like the spectral slope and E2/E3 ratio. The spectral slope describing the approximate exponential decline in chromophoric DOM (CDOM) absorption with increasing wavelength is widely used for tracing changes in the chemical composition of CDOM.[6; 7] E2/E3 is the ratio of absorbance at 250 nm to at 365 nm and often used as an indicator for humification and molecular weight of humic substances.[8-10] The lower values of E2/E3 ratio may be indicative of the presence of structures with higher molecular weight, aromaticity, and humification degree.

Not all molecules in DOM interact with light. CDOM is defined as the light-absorbing fraction of DOM ([DOM]>[CDOM]) and is the main absorber of light in environmental systems.[11-14] Thus, employing absorbance as a surrogate for the physicochemical properties of DOM (e.g., molecular weight) implies the sometimes arbitrary assumption that the behavior of the chromophores represents the behavior of either the most important components for a specific

application (e.g., relationship between $SUVA_{254}$ and formation of disinfection byproducts), or directly correlates with how the rest of the mixture behaves.

The exponential shape of DOM UV-Vis absorption spectra is widely observed regardless of source and usually is featureless, but some shoulders or peaks can be observed for example for organic matter from atmospheric sources,[15] from algae provenance,[16] or through Gaussian decomposition of DOM spectra.[17] Two alternative theories have been proposed to explain DOM absorbance spectrum. The first one postulates that the absorbance is the sum of the individual DOM chromophores absorbance. The second model postulates that the absorbance is the sum of two terms: 1) the sum of the absorbance of the individual chromophores and 2) a term due to charge-transfer (CT) interactions between electron donor (mostly phenols) and acceptor (mostly quinones and ketones) moieties of DOM, that contributes to the absorption at wavelengths ≥ 350nm. The effects of sodium borohydride reduction on DOM UV-Visa absorption spectra were often used to probe into the CT model. The reduction transforms quinones and ketones functional groups into phenols, decreasing so the amount of CT interactions.[18-21] We refer the reader to recent publications, which describe alternative and complementary mechanistic interpretations for the shape of the UV-Vis spectra of DOM.[21-27]

The aforementioned CT interactions were assumed in the literature to be *intra* molecular interactions due to DOM absorption spectra being concentration independent, but CT interactions can in principle be due to both *intra* and *inter* molecular interactions. *Inter* molecular CT interactions were the scope of a previous work that indicated formation of π-stacking interactions in Suwannee river fulvic acid (SRFA) models, with subsequent effects on the calculated absorbance spectra.[28] These results offer computational confirmation of CT interactions within DOM, suggesting that they contribute partially to its optical properties. However, it was shown

88 that the formation of π-stacking clusters occurred in water, but that switching the solvent to non-
89 polar ones resulted in disruption of the π-stacking structures as well as the whole molecular
90 assembles.[28] This result further highlights the dynamic nature of these assemblies. Consequently,
91 in non-polar solvents the formation of CT complexes via π-staking clusters is insignificant and
92 cannot contribute to absorption maximum ($\lambda_{a,max}$) of UV-spectra. As DOM spectra are mostly
93 solvent independent,[24] this raises the question of whether these inter molecular CT interactions
94 contribute significantly to DOM absorbance. *Intra* molecular CT interactions were postulated to
95 exist based on spectrofluorometric observations and also on the effects of sodium borohydride
96 reduction on DOM absorbance and fluorescence properties.[18; 23] These observations rely on bulk
97 DOM properties and with limited insight on what is happening at the molecular level. The
98 possibility of calculating the UV-Vis spectra of molecules allows to test for the possibility of *intra*
99 molecular CT interactions and on which conditions such interactions should take place.

100 Recently it was shown that time – dependent density functional theory (TD-DFT) method
101 reproduces very accurately optical susceptibilities for a wide range of organic compounds that
102 could be found in DOM.[29; 30] TD-DFT is a first-principles method without any empirical
103 spectroscopic parameters. The calculation of transition energies from time-dependent density
104 functional linear response theory has been described in details by Neese.[31] The linear response
105 approach directly yields the transition energy rather than the total energies of the ground- and
106 excited states. Thus, the excited states themselves are never explicitly calculated. Rather, their
107 energies are deduced from the poles of a frequency dependent ground state property. Thus, for the
108 ground state all properties can be calculated from the analytic derivatives of the total energy. The
109 same procedure applies to the excited states as well. The total energy of the excited state is simply

110 the sum of the ground state energy and the transition energy predicted by the TD-DFT procedure.
111 The derivatives of this total energy then define all excited state properties.

112 The main objective of this study was to use computational chemistry tools to conduct a
113 detailed evaluation of the UV-Vis spectra of DOM. Specifically, TD-DFT was used to calculate
114 the UV-Vis spectra for a selection of chromophores chemically similar to those chromophores that
115 could be expected in DOM. Calculated spectra were summed together in a superposition-type
116 approach for comparison to DOM absorbance spectra. Additionally, we evaluated whether certain
117 concentration conditions could give rise to *inter* molecular CT interactions being concentration
118 independent. Finally, TD-DFT was used to calculate the spectra of a selection of compounds that
119 should exhibit *intra* molecular CT interactions to evaluate in which conditions these CT
120 interactions should occur.

MATERIALS AND METHODS

Generation of DOM Models

In this work, five models (numbered 1 to 5) representing Suwannee River fulvic acid (SRFA) were used. Each model contains a number of molecules, each assigned to a letter (e.g., for model #1, molecules a to m, see Table S1). SRFA was chosen as representative of river headwater allochthonous DOM from the International Humic Substances Society, and because it is in all likelihood, the most studied DOM. The models were created on the basis of SRFA chemical characteristics[32] using principles proposed by Vialykh et al.[33; 34] The algorithm of fragment selection and s*creening Criteria* of each model were described in Vialykh et al.[28] Specific chemical species were selected for use in this study. These structures are shown in Table S1 of the Supporting Information (SI). The number of each fragment in the models was equal one. Table S2 includes the elemental composition for each model, as well as the lowest, and highest molecular weight for the components in the models. Lastly, the mean molecular weight for the models is included. The number average molecular weight for SRFA has been estimated at 724 ± 68 Da based on vapor pressure osmometry,[35] 610-760 Da based on hydroxyl radical reactivity,[36] 968 Da based on size-exclusion chromatography data[37] while the latest high-resolution MS data showed that the range of molecular masses of aquatic humic substances is 290-600 m/z.[38] Though we attempted to build the models that would reflect the latest data on average molecular weight of molecules present in SRFA, the computational restrictions (time and cost) force us to generate models with the mean molecular weight on the lower end of these estimates (~300-400Da). Larger chromophores can potentially move the absorption band more into the visible as DOM size fractionation experiments indicate that the larger fraction absorbs relatively more visible light than the smaller fractions.[39]

144

145 **Absorbance Spectra Calculations**

146 First, the geometry optimization of each molecule was performed by DFT calculations. The
147 properties of a many-electron system can be determined by using functionals, i.e., functions of
148 another function. In the case of DFT, these are functionals of the spatially dependent electron
149 density.

150 Further TD-DFT calculations were performed to obtain UV spectra of selected molecules.
151 TD-DFT is a quantum mechanical theory that allows to investigate the properties and dynamics of
152 many-body systems in the presence of time-dependent potentials, such as electric or magnetic
153 fields. The effect of such fields on molecules can be studied with TDDFT to extract features like
154 excitation energies, frequency-dependent response properties, and absorption spectra.

155 The ORCA 4.0.1 package[40] was used to carry out the geometry optimizations and spectral
156 calculations for individual molecules. Calculations were performed for both fully protonated
157 molecules, that correspond to pH 1-2, and with deprotonated carboxylic groups, which corresponds
158 to pH ~5. The geometry optimizations were performed by using the B3LYP functional with def2-
159 TZVP basis set in water solvent with SMD solvation model. Tight self-consistent field
160 convergence criteria were set without symmetry constraints. The RIJCOSX approximation was
161 used with auxiliary basis def2/J to accelerate the calculations without notable loss of accuracy. The
162 TD-DFT and sTD-DFT calculations were performed by using B3LYP or BP86 functional on the
163 DFT-optimized structures with def2-TZVP or aug-cc-pVDZ basis sets. The RIJCOSX
164 approximation was employed to speed up the calculations. SMD solvation model was used to
165 conduct the calculations in water solvent. The calculation of the charge transfer in the excited
166 states has been performed by the TheoDORE program package.[41; 42] To plot the absorption spectra

167 for individual molecules, Avogadro program[43] was used with Gaussian line shape and peak width
168 20. The increase in peak width above 20 resulted in smoothing the curve and disappearing peaks,
169 e.g., peak at 260 nm for flavone (Figure S1). In order to plot the absorption spectra for a mixture
170 of several molecules, the Octave[44] script was used to calculate Gaussian line shape of absorption
171 spectra with peak width 20. The calculated spectra of coumarin and flavone was compared to their
172 measured spectra to verify the accuracy of the calculation (Figure S1).

173 UV-Vis spectra for the different models were calculated based on the superposition model,
174 *i.e.,* we assumed that there were no interaction between individual molecules that would lead to
175 additional absorption bands, and the overall spectrum of the model was calculated as a sum of
176 spectra of individual molecules. Additionally, a global model containing all molecules was also
177 calculated (see Table S1 for the structures presents in each model). For different pH the spectra
178 were calculated separately.

179 Many molecules were used to create a computational model. Some of these molecules are
180 difficult to purchase in pure form or not available commercially, making the comparison of the
181 calculated spectra with spectra of real mixture of molecules not possible.

182 **Chemicals and Solutions**

183 SRFA (catalogue number 1S101F) was obtained from the International Humic Substance
184 Society (IHSS, St-Paul, MN, USA). Coumarin and flavone (purity min. 99%) and HPLC grade
185 methanol were obtained from VWR. All solutions were made using ultrapure water (resistivity
186 18.2 MΩ cm) obtained from a Sartorius Arium pro dispenser or equivalent. The SRFA solution
187 was made according to the methods presented in Leresche et al.[45] UV-Vis absorbance spectra were
188 measured on a Cary 100 Bio UV-visible spectrophotometer using a 1 cm path length quartz
189 cuvette.

190

191 **Borohydride reduction**

192 To simulate the effects of borohydride on our model compounds, we applied the following
193 transformation rules: acetophenone to 1-phenylethanol, benzophenone to the corresponding
194 alcohol, esters to the corresponding cleaved alcohol, anthraquinone to anthracene, unconjugated
195 ketones and aldehydes to the alcohol, and conjugated ketones and aldehydes to a mix of conjugated
196 and unconjugated alcohols. Please see Table S1 for the structures of the reduced compounds.

197

198 **RESULTS & DISCUSSION**

199 **Influence of Functional Groups and Chemical Structures on UV-Vis Spectra**

200 It is known that the presence of different functional groups or molecular fragments affects
201 UV-Vis spectra,[46] and because DOM contains a range of functional groups, this can extend the
202 absorption of chromophores into the visible region. Light absorbed in the UV-Vis range induces
203 an electron shift to one of the empty molecular orbitals. For the wavelength range above 220 nm,
204 most absorption occurs from extensive conjugation that decreases the energy gap between the
205 highest occupied molecular orbital (HOMO) and the empty molecular orbitals. For example,
206 benzene has a $\lambda_{a,max}$ at ~254 nm, whereas for naphthalene the value is 275 nm, and 356 nm for
207 anthracene (the sequence of linear poly-aromatic hydrocarbons has a shift in wavelength max of
208 ≈75 nm per ring). In the case of phenol, $\lambda_{a,max}$ is 270 nm, and 262 nm for methylbenzene. As we
209 consider the UV-Vis spectrum of DOM, and the fact that it extends into the visible, it is expected
210 that single ring components will dominate the absorption below 300 nm while in the visible multi-
211 ring chromophores are the main light absorbers. This can be observed in the present data set (Table
212 S4 and Figure S2) were most molecules absorbing at wavelengths longer than 400 nm have multi-
213 ring chromophores while molecules having their $\lambda_{a,max}$ in the 250-300 nm range are mostly single-
214 ring compounds.

215 Flavones are plants pigments and potentially a class of DOM chromophores.[47] Spectra
216 calculation for a series of flavones molecules substituted with various electron donating or
217 withdrawing groups showed that the substituents shift the $\lambda_{a,max}$ by up to 120 nm (Table S5 and
218 Figure 1). The Hammett σ constants (that relate a functional group to its electron donating or
219 withdrawing character) vs $\lambda_{a,max}$ relationships follows a U-shape non-linear relationship with
220 shorter $\lambda_{a,max}$ values for substituents having σ values close to 0 and longer $\lambda_{a,max}$ values for electron

221 poor and electron rich substituents. This observation is similar to the one made in a study for
222 substituted squaraine dyes[48] but differs from the results of a study on substituted triphenylamines
223 were a linear relationship was observed between σ and $\lambda_{a,max}$.[49] The U-shape can be rationalized
224 by the absorbance spectra having a relatively important absorption band around 300 nm and for
225 some of the substituents to present additional absorption band at longer wavelengths that shift
226 $\lambda_{a,max}$ (Figure 1). Note that if there are more than one absorption maxima, $\lambda_{a,max}$ corresponds to the
227 longest wavelength maxima. The wavelength of maximum absorption of the 300 nm feature (λ_M)
228 can be seen to follow a linear relationship with the σ substituent (Figure 1) and it can be concluded
229 that the observed U-shape relationship between $\lambda_{a,max}$ and the Hammett σ substituent comes from
230 the appearance of additional absorption bands for some of the compounds.

231 Analysis of UV-Vis spectra by the region of $\lambda_{a,max}$ revealed that molecules containing
232 quinone groups have $\lambda_{a,max}$ above 400 nm (Table S4). For example, 2,3-dicarboxy-1,4-
233 benzoquinone has a $\lambda_{a,max}$ at 611 nm in deprotonated form and at 506 nm in protonated form. The
234 presence of three conjugated aromatic rings (with or without functional groups) results in $\lambda_{a,max}$
235 above 400 nm as well. The presence of ketone groups conjugated with an aromatic ring result in
236 $\lambda_{a,max}$ by the 300-400 nm region. Presence of two or more conjugated double bonds and COOH
237 group also results in $\lambda_{a,max}$ between 300-400 nm. Molecules containing a single aromatic ring with
238 different functional groups (except ketone) tend to have $\lambda_{a,max}$ between 250-300 nm. $\lambda_{a,max}$ in the
239 same range was observed for molecules with two conjugated double bonds.

240 DOM being a mixture of compounds, its absorbance spectrum reflects the spectra of the
241 individual components. For the aforementioned superposition model, DOM spectrum is simply the
242 sum of the spectra of the individual components and one can model DOM spectrum by averaging

the individual components. For the CT model, one must add to the spectra average a term corresponding to CT interactions. Investigations on these CT interactions are presented below.

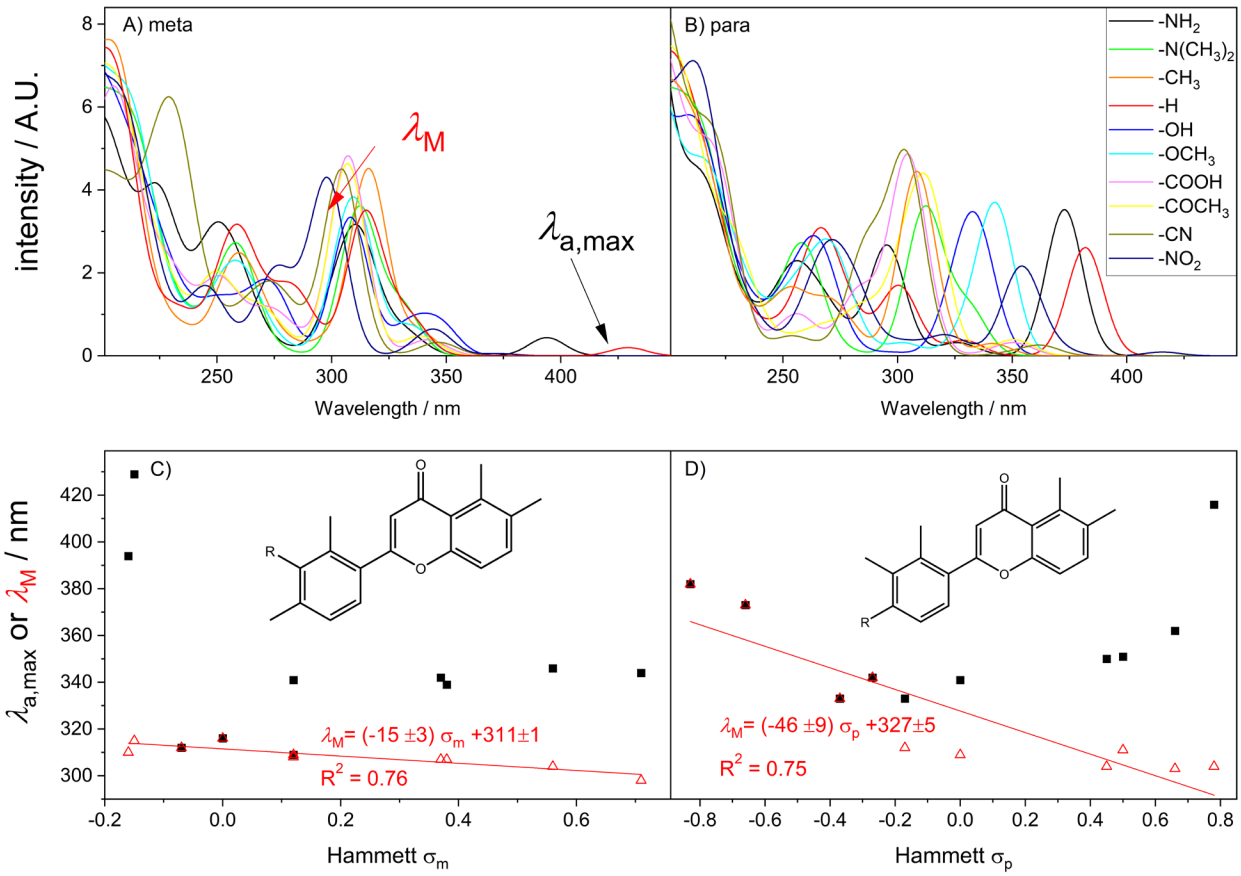

Figure 1. Calculated absorbance spectra for the substituted flavones in the A) meta and in the B) para position. Absorption maximum wavelength ($\lambda_{a,max}$) and absorption maximum wavelength for the peaks centered around 300 nm (λ_M) of a series of flavones backbone substituted molecules in the C) meta and in the D) para position. The substituents are presented in Table S4.

Simulated UV-Vis Spectra of the SRFA models

The UV-Vis spectra of the models were created by averaging the UV-Vis spectra of the models' molecules (see above). Since the real samples of DOM contain thousands of individual molecules and our models contained 8-21 molecules and 65 for the global model, the quantitative comparison is not feasible. Thus, only qualitative comparison between calculated and experimental UV-spectra was performed. UV-Vis spectra calculated for the models decayed with increasing wavelength. The shape of the spectra was close to exponentially decaying curve as the absorption

258 spectrum of SRFA (Figure 2). Although all models include molecules that absorb light in a region
259 above 400nm, the calculated UV-Vis spectra for models #4 and 5 were the closest to the
260 experimental data, whereas spectra for model #2 had the largest discrepancy with experimental
261 data. The observed variation in the UV-Vis spectra between models might be a result of the mean
262 molecular weight of the models. Thus, for models #4 and 5 these values were 497 and 391Da
263 accordingly, since significant part of the molecules included in the models had large molecular
264 weight (above 400Da) and in the structure of each molecule there were several conjugated groups
265 that absorb light, which produces a broadening of the individual absorption peaks and additionally
266 contributes to increase of absorption at longer wavelengths. The opposite could be said about
267 model #2 that is composed mainly from small molecules with molecular weight below 260Da.
268 Though there were fragments that absorb above 400 nm (pH1) and 600 nm (pH5) the number of
269 fragments that did not absorb light above 250 was significantly higher than in other models, e.g.,
270 seven fragments in model#2 vs one fragment in model #4. The spectra for the other molecules in
271 model#2 were presented as a line with one or two individual sharp absorption peaks, rather than a
272 smooth exponentially decaying curve. As a result, a larger discrepancy between UV-spectra
273 calculated for model#2 and experimental data was observed in the range between 250-400 nm.
274

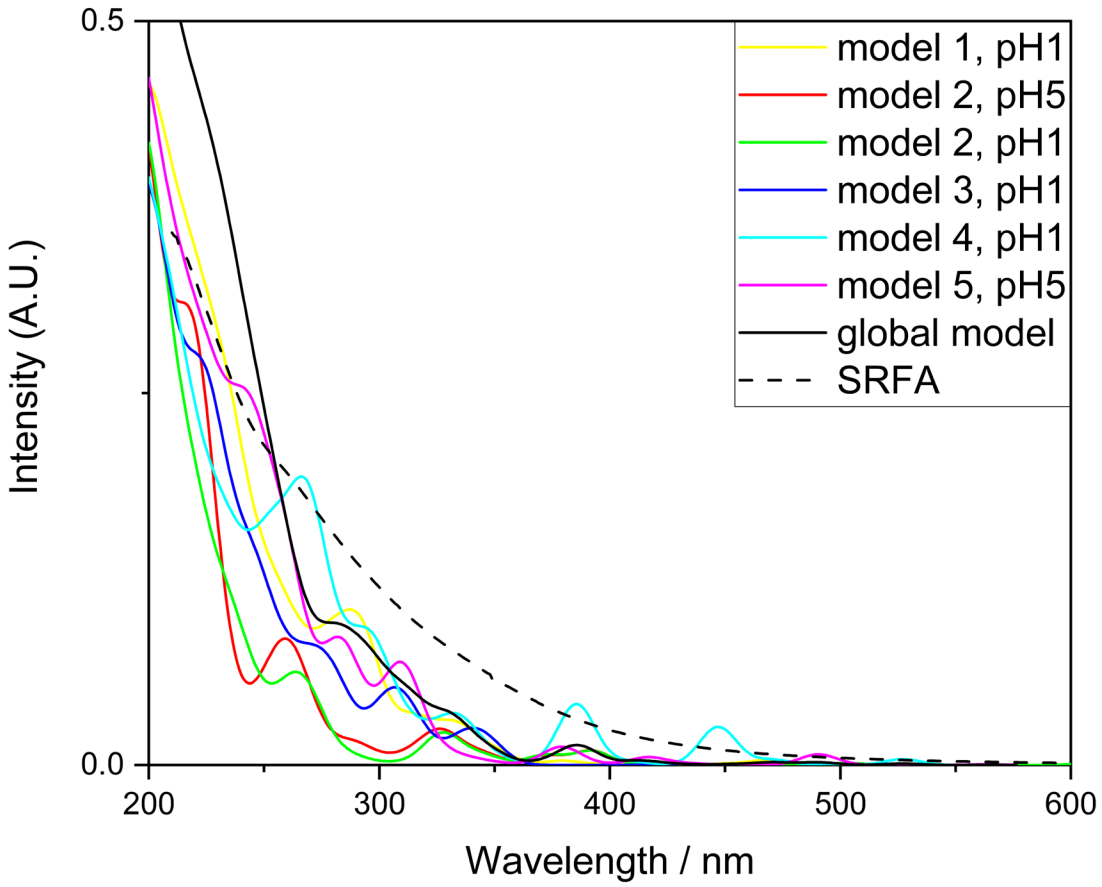

Figure 2. UV-Vis spectra of Suwanee River Fulvic Acid (SRFA) (dashed line) measured at pH 7, of the 5 simulated models (continuous lines) and of the global model (that contains all the 5 models).

It can be observed that the models' absorbances decrease at longer wavelength and that absorption peaks are observable. These peaks are likely due to the absorbance of a single model compound and would likely vanish if many more compounds would be included in the models. Indeed, the global model that includes all the models does not present pronounced peaks (Figure 2). Comparing the model's spectra to the one of SRFA, it is possible to see that the model's absorbance decreases faster than SRFA with increasing wavelength. This discrepancy could be due to the mean molecular weight of the models being lower than the one of SRFA (Note, for

287 computational time reasons, it is not actually possible to calculate the absorbance of molecules
288 having molecular weights above ≈800 Da). The high molecular weight fractions of SRFA are
289 known to absorb relatively more in the visible than the low molecular weight fractions[39] and the
290 calculated models are probably more representative of the low molecular weight fractions of
291 SRFA.

292 **Evaluation of Charge-Transfer interactions**

293 *Inter molecular charge-transfer interactions*

294 It should be noted that the absorbance spectra calculated in the present article only include
295 the individual components' contributions and would not integrate any *inter* molecular CT
296 interactions. The current working model for DOM charge-transfer interactions is that they exhibit
297 structural similarities to eumelanin (a pigment that protects the skin against sunlight [50]) in terms
298 of their three-dimensional configuration. The absorbance of eumelanin-like compounds presents
299 a CT complex absorbance in the visible spectra that also has the particularity to be concentration
300 dependent.[51] By contrast, DOM absorbance spectra are concentration independent. This raises the
301 question of whether conditions exist such that *inter* molecular interactions do not exhibit a
302 concentration dependence. This was evaluated using the following model: the equilibrium
303 equation for the formation of a CT complex between a DOM electron acceptor and donor can be
304 written as $A+D \rightleftharpoons CT$ with A and D an electron acceptor and donor respectively, CT the charge-
305 transfer complex and *K* the corresponding equilibrium constant. For CT to be [DOM] independent,
306 [CT] should be directly proportional to [DOM]. Note, we chose a criterion where less than 10%
307 variation is not considered to be a significant change, this choice is arbitrary, but we do estimate
308 that this corresponds to the limit of what could be detected by absorbance measurements of DOM

for wavelengths ≥400nm. See Text S1 for the derivation of the reaction formula and Table S7 for the presentation of the evaluation results for several $[A]_0/[D]_0$ ratios and various values of *K*.

The evaluation results indicates that for the $[A]_0/[D]_0$ ratios values of 0.01 and 0.1, *inter* molecular interactions would exhibit a concentration dependence for equilibrium constant below ≈1000 (corresponding ΔG = -17.1 kJ mol^{-1}) while above such number the concentration dependence would be negligible. For the equimolar $[A]_0/[D]_0$ ratio, *inter* molecular interactions would exhibit a concentration dependence for equilibrium constant below ≈10000 (corresponding ΔG = -22.8 kJ mol^{-1}). For comparison with these ΔG values, a water hydrogen bond has an energy of -21.6 kJ mol^{-1} (Note, this value is per mol of water molecules and corresponds to a value of -10.8kJ mol^{-1} of hydrogen bond).[52] Overall, these calculations indicate that in order to not exhibit concentration dependency, two molecules have to be bonded through either two bonds with strength equivalent to hydrogen bonds or more than two less energetic bonds. As DOM spectrum is concentration independent, this exercise indicates that if there is any *inter* molecular CT complexes in DOM, the molecules need to interact relatively strongly. Our previous work suggest that the probable main mechanism for intermolecular CT is π-stacking.[28] For usual H-bonds, namely X-H----Y with nitrogen or oxygen as X and Y, the binding strength is about -17 to -27 kJ mol^{-1}.[53] At the same time π-π stacking between two single aromatic rings is -10 to -12 kJ mol^{-1},[54] clearly in usual case H-bond is evidently stronger. However, there are other situations where H-bond may also be quite weak (e.g. C-H----O, whose binding energy is lower than -4 kJ mol^{-1}), while π-π stacking may also be quite strong (e.g. cyclo[18]carbon dimer, the binding energy of which is about -38 kJ mol^{-1}).[55] Additionally, the combination of both π-π stacking and H-bonds could prevent π-stacking aggregates from dissociation.

332 *Intra molecular charge-transfer interactions*

333 To assess for the possibility of *intra* molecular CT, the spectra of molecules that could
334 undergo *intra* molecular CT were calculated (Figure 3A). These molecules were constructed using
335 a flavone or a coumarin tetra-methyl substituted backbone. Then each methyl position was
336 alternatively replaced by a (CH_2)n-hydroxybenzene (n= 2 or 3) for the coumarin backbone or
337 (CH_2)n- dihydroxybenzene for the flavone backbone. As negative controls, (CH_2)n-
338 methylbenzene and (CH_2)n-dimethylbenzene were substituted to the hydroxybenzene and
339 dihydroxybenzene respectively. Additionally, the spectra of molecules known to exhibit
340 unconjugated CT interactionss[22] were also calculated (molecules 8, 9a and 9b). In these molecules
341 the CT might occur due to π-staking interactions between non-conjugated aromatic rings.
342 Molecules used in biological imaging that possess fluorescence properties assigned to conjugated
343 *intra* molecular CT complexes[56; 57] were also calculated (Figure 3B). The donor and acceptor in
344 these molecules are connected via conjugated backbone (e.g., alternation of single and double
345 bonds) resulting in CT via delocalized π-orbitals. These molecules possess an electron acceptor
346 part (1-benzopyran-4-one) and an electron donor part (benzene ring) that was substituted in the
347 para position with diverse electron rich $(N(CH_3)_2$, OH, $OCH_3)$ functional groups and for controls
348 an electron poor functional group (NO_2) and a H substituent.

349

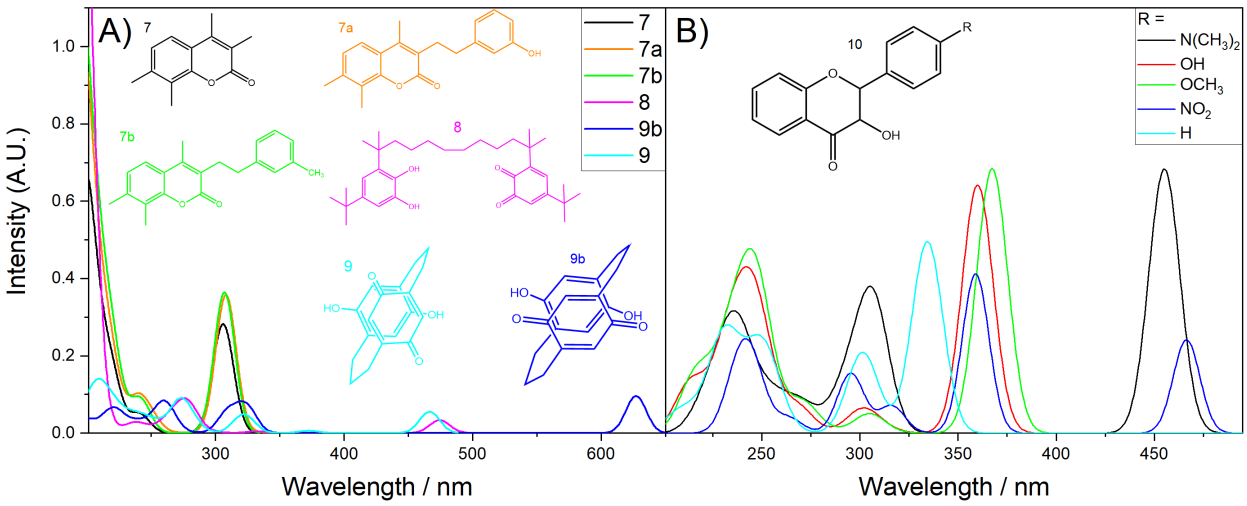

Figure 3. Structure and calculated absorbance spectra of the compounds investigated for *intra* molecular charge-transfer (CT) interactions. A) molecules investigated for unconjugated *intra* molecular CT interactions. B) molecules investigated for conjugated *intra* molecular CT interactions. Note, Figure S4 presents additional compounds to Figure 3A substituted on the substitution of the other methyl groups of the coumarin as well as similar compounds based on a flavone backbone. Figure S5 presents additional compounds to Figure 3B having the coumarin backbone hydroxyl group replaced by either a hydrogen atom or a -OCH_3 group.

The absorbance spectrum of molecule 8 measured in acetonitrile presents an absorbance band between 500-600 nm that was assigned to a CT complex.[58] The calculations fail to capture this 500-600 nm band (Figure 3A) with the calculated spectra only slightly different from the spectra of the dihydroxybenzene and quinone subunits (Figure S3). The reasons for this discrepancy could be the difference in solvent; water being a protic polar solvent can make hydrogen bonds with the hydroquinone and quinone moieties of molecule 8 that acetonitrile would not. The water hydrogen bonds would compete with the formation of *intra* molecular CT complex, and it is plausible that molecule 8 only exhibits CT properties in an aprotic solvent. An alternative explanation is that the assignment of the CT complex to *intra* molecular was not correct and that the observed 500-600 nm $\lambda_{a,max}$ was due instead to *inter* molecular CT complex. The spectrum measured in dioxane of molecules 9 presents a weak absorption band centered around 500 nm attributed to *intra* molecular CT interactions while for molecule 9b a strong CT absorption band

371 is visible at 350-600nm.[59] The calculated spectrum of molecule 9b presents an $\lambda_{a,max}$ at λ=630 nm
372 that can be attributed to *intra* molecular CT interactions (Figure 3A) while for molecule 9 a less
373 intense $\lambda_{a,max}$ can be observed at λ=470 nm that can also be attributed to *intra* molecular CT
374 interactions. We also calculated molecules similar to molecule 9b with various carbon atoms (n=2-
375 9) between the two rings, the increase in carbon atoms increased the distance between the two
376 rings. The results of the calculation are presented in Figure S3 and indicate that CT is observed
377 only for n= 2 or 3, when the distance between two rings less than 5Å while for n ≥4 no CT is
378 observed.

379 For the coumarin and flavone backbone molecules grafted with hydroxy or dihydroxy-
380 benzene groups, none exhibited non-conjugated CT absorption band (Figure 3A and S4). One
381 possible explanation is that the formation of *intra* molecular CT complexes is competing with the
382 water hydrogen bonds and that the formation of such CT is not favorable in water. As molecule
383 9b presents some CT absorption properties, it could indicate that to present CT properties in water,
384 molecules have either to be constrained in their shape in a way that allows π-stacking formation
385 or that *intra* molecular CT complexes have to outcompete water hydrogen bonds. Overall, the
386 calculations indicate that intramolecular CT between non-conjugated molecular parts would
387 probably depend on π-stacking, between two or multiple aromatic rings in close proximity.

388 For the flavone substituted molecules investigated for conjugated *intra* molecular CT
389 complex, (Figure 3B and S5), $\lambda_{a,max}$ was of ≈455 nm for the $N(CH_3)_2$ group, ≈370 nm for the OH
390 and OCH_3 groups and ≈510 nm for the control electron withdrawing NO_2 group and ≈356 nm for
391 the H group with mean CT contribution to the singlet excited state of 69%, 44%, 50%, 77% and
392 30% for the $N(CH_3)_2$, OH, OCH_3, NO_2 and H group respectively. These results indicate that
393 intramolecular CT interactions are affected by the substitution of electron donor or acceptor groups

394 in conjugation with the chromone moiety. The occurrence of an electron donating $–OCH_3$ or -OH
395 groups in the para-position of the phenyl ring mildly enhances the charge transfer by 4-25% (Table
396 S8) compared to control molecule where R- is hydrogen. The spectral response is qualitatively
397 similar to the hydrogen control molecule ($\lambda_{a,max}$ red shift of up to 44nm). The presence of an
398 electron donating $–N(CH_3)_2$ group causes an increase of CT up to 50% and red shift of $\lambda_{a,max}$ up to
399 134 nm resulting in a new spectral peak in the visible region above 400 nm. Interestingly electron
400 withdrawing $–NO_2$ group in the same position opens competing charge transfer channels that cause
401 a new spectral peak with $\lambda_{a,max}$ 480-510 nm and higher CT contribution (75-81%).Thus, $-OCH_3$
402 or -OH groups didn't induce absorption in the visible range except for the $N(CH_3)_2$ group while
403 the control molecule (NO_2) possessing two electron accepting parts showed red shifted absorption.
404 This result is similar to what was observed for substituted β-enaminones where the molecule
405 having two electron accepting parts had an absorption spectrum that was red shifted compared to
406 the molecule having an electron accepting and an electron donating part.[60]

407 **Effects of sodium borohydride reduction**

408 *Sodium borohydride reduction*

409 Sodium borohydride DOM reduction has been used by many [18; 20; 21; 61-70] for investigations
410 on DOM absorption and fluorescence properties. The calculation of the borohydride reduction
411 products of the compounds selected in our models is possible. This allows us to evaluate the effects
412 that borohydride reduction should have on our model's absorbance properties, which are based
413 uniquely on the superposition of individual chromophores. One difficulty doing such exercise is
414 the prediction of the correct reduction products.

415 Borohydride reduction was presented originally in the environmental chemistry literature
416 as mainly reducing carbonyls groups to alcohols within DOM.[18; 71] This is probably too simplistic

417 since additional side reactions can take place, e.g., for α,β-unsaturated aldehydes and ketones, the
418 reduction of double bonds adjacent to the carbonyl group was seen to take place leading to the
419 formation of a mixture of the saturated and the unsaturated alcohol.[72] Esters are potentially also
420 reduced under large borohydride excess conditions.[73] The experimental conditions proposed for
421 DOM reduction are a 25-fold borohydride mass excess for 2-4 days of reaction,[71] which probably
422 allows for reaction of some ester moieties within DOM. Identification of the borohydride reduction
423 products confirms that the reduction is not limited to the conversion of carbonyls groups to
424 alcohols. For example, three rings opening products (one unsaturated and two saturated) are
425 obtained upon coumarin's borohydride reduction,[74] anthrones or anthracenes are obtained upon
426 reduction of substituted anthraquinones,[75] and dihydro esters are the reduction's products of a
427 series of methyl (*p*-substituted phenyl)-acrylates.[76] We adopted the rules presented in the
428 experimental section to calculate the different products of borohydride reduction. The molecules
429 before and after reduction are presented in Table S1.

430 *Individual molecules*

431 In most cases, borohydride reduction of individual molecules leads to a blue shift in their
432 UV-Vis spectra (Figure 4), however, a red shift after reduction was observed for several molecules
433 (e.g., molecules **c** and **m** in model #1; molecules **e** and **f** in model #3 and molecule **k** in model #5,
434 see Table S1 for the molecules before/after reduction). The blue shift in $\lambda_{a,max}$ varies for different
435 molecules and was between <1 nm to 317 nm at pH 1 and between 8 nm to 364 nm at pH 5,
436 whereas the red shift was between 3.5 nm to 66 nm at pH 1 and between 16 nm and 29 nm at pH
437 5. These results are similar to the one observed upon borohydride reduction of a series of model
438 quinones where a blue shift in $\lambda_{a,max}$ was observed for all but one of the quinones (anthraquinone-
439 2,6-disulfonate) following borohydride reduction.[18]

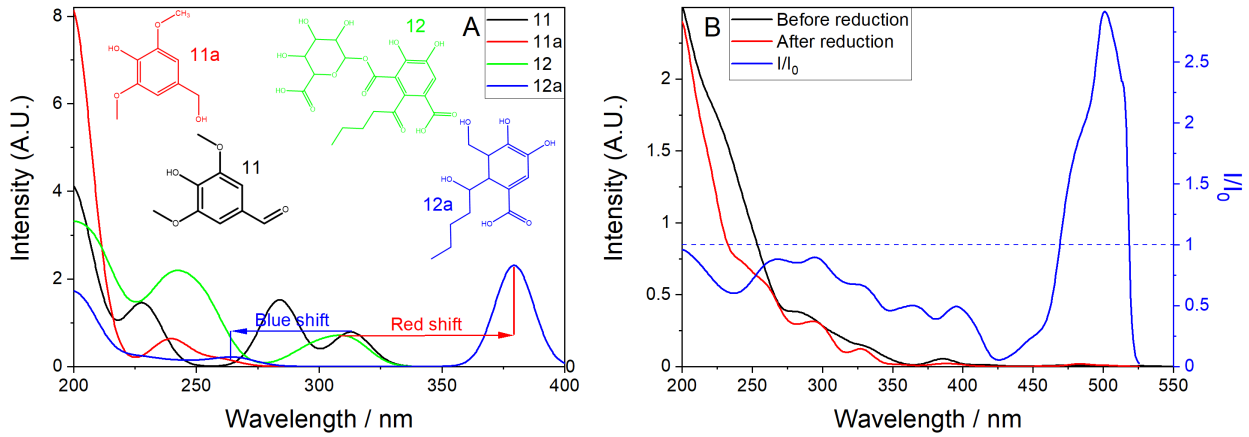

Figure 4. Effects of sodium borohydride reduction on the absorbance spectra. A) structure and calculated absorbance spectra of the parent molecules (11 and 12) and of the borohydride reduced products (11a and 12a). B) Calculated UV-Vis absorbance spectra of the global model before (black) and after (red) borohydride reduction (at pH5) and absorbance ratio (blue, I/I_0). The absorbance ratio was smoothed using a 30 points (≈25nm) adjacent averaging algorithm.

Effects of sodium borohydride on the spectra

For the global model, a blue shift after reduction was observed with a $\lambda_{a,max}$ change of 25 nm (pH1) and 123 nm (pH5) (Table S9). At the same time for models #1 and #3 a red shift in $\lambda_{a,max}$ was observed at pH1. The largest blue shift in $\lambda_{a,max}$ (237 nm at pH5) was observed in model #2 which were composed from small fragments with molecular size between 120-260 Da, whereas for models #4 and #5, composed mostly from fragments with molecular weight above 350 Da, the blue shift was much lower, 24 or 69 nm and 12 or 60 nm at pH 1/pH5, accordingly. Thus, borohydride reduction could significantly decrease the $\lambda_{a,max}$ of small molecules due to destruction of quinone groups, whereas the reduction had lesser effects on the $\lambda_{a,max}$ of molecules with more complex structure and molecular weight above 400 Da.

UV-Vis spectrum calculated for the global model (Fig 3B) indicates that borohydride reduction decreased the absorbance, a trend similar to the experimental results.[18] The calculated relative decrease in absorbance (I/I_0) is similar to the measured one with a decrease that is more marked at longer wavelength in the 200-400 nm region. The only area that diverges from this

461 behavior is in the 480-520 nm range. The divergence comes most probably from the very low
462 intensity measured in this wavelength range. Overall, our results indicate that the superposition
463 model could also explain well the effects of borohydride reduction on DOM absorbance spectra
464 not only the CT model as postulated in Ma et al.[18]

465 **ENVIRONMENTAL IMPLICATIONS**

466 The work presented here continues the development of computational tools to assess the
467 origins of the optical properties of DOM. Computational approaches offer an advantage when
468 evaluating the superposition model for understanding DOM's optical properties since transitions
469 can be determined computationally for compounds not commercially available. The work
470 presented herein indicates that a superposition of chromophores is largely able to reproduce the
471 absorbance spectral shape and effects of borohydride reduction. These spectral properties have
472 previously been argued to be consistent only with a charge-transfer model, and a recent study
473 highlights that this behavior is also consistent with the behavior of a model charge-transfer
474 complex (quinhydrone).[27] Therefore, the absorption properties of DOM and their responses to
475 borohydride reduction appear to be consistent with both a superposition model and charge-transfer
476 model.

477 One aspect of the relationship between CDOM and DOM that still requires clarification is
478 the overall mass ratio between both, [CDOM]/[DOM]. It is expected that this ratio will be less
479 than unity, as not all components of DOM will absorb. In the case of SFRA, we can use the
480 developed models to ascertain what this ratio would be. Given that DOM is mostly quantified in
481 terms of carbon concentration, we use carbon ratios to ascertain the value for [CDOM]/[DOM].
482 Table S10 shows our calculated values. The procedure to obtain this value was based on defining
483 a chromophore as a series of consecutive sp^2 hybridized carbon units, including oxygen atoms

484 bonded to sp^2 carbons. Figure S6 shows an example of the delineation used. We did this only for
485 chromophores that would absorb at wavelengths above 260nm. As shown in Table S10, the ratio
486 of [CDOM] to [DOM] is roughly 53%, indicating that a little more than half carbon atoms are
487 attached to a chromophore. This would translate into ~53% of the DOC in SFRA being
488 chromophoric. This number can be compared to the ^{13}C nuclear magnetic resonance distribution
489 from the IHSS website,[77] for SRFA (catalogue number 1S101F) the fraction of carbonyl, carboxyl
490 and aromatic SRFA carbons is 51%, which is a number close to the 53% calculated here. It should
491 be noted that not all carboxylic groups should be part of a chromophore and that the 51% should
492 be considered as an upper limit maximum.
493

Acknowledgements

Partial funding for this study came from the US National Science Foundation (CBET #1453906) and from Bio Huma Netics, Inc (Lyndon W. Smith and Richard Lamar). This work utilized resources from the University of Colorado Boulder Research Computing Group, which is supported by the National Science Foundation (awards ACI-1532235 and ACI-1532236), the University of Colorado Boulder, and Colorado State University. The authors would like to acknowledge Garrett McKay for his excellent contributions to this work.

Associated Content

Supporting information

The supporting information is available free of charge on the ACS website at DOI:

The supplemental information includes further figures, tables and text sections detailing the models' chemical structures, the effects of sodium borohydride on the structures, the molecules absorption by wavelengths, the effects of substituents on the absorption maximum, the estimation of *inter* molecular CT interactions, additional compounds investigated for *intra* molecular CT interactions and an example of the calculation of the chromophoric part of a structure.

Author information

Corresponding author

*E-mail: Frank.Leresche@Colorado.edu

ORCID

Elena Vialykh: 0000-0001-7351-6567

Frank Leresche:0000-0001-8400-3142

Fernando L. Rosario-Ortiz: 0000-0002-3311-9089

Note

The authors declare no competing financial interest.

References

1. Thurman EM. 2012. *Organic geochemistry of natural waters*. Netherlands: Springer Netherlands. 2012. 312-324.
2. Weishaar JL, Aiken GR, Bergamaschi BA, Fram MS, Fujii R, Mopper K. 2003. Evaluation of specific ultraviolet absorbance as an indicator of the chemical composition and reactivity of dissolved organic carbon. Environmental Science & Technology. 37(20):4702-4708.
3. Shutova Y, Baker A, Bridgeman J, Henderson RK. 2014. Spectroscopic characterisation of dissolved organic matter changes in drinking water treatment: From PARAFAC analysis to online monitoring wavelengths. Water Research. 54:159-169.
4. McKay G, Huang WX, Romera-Castillo C, Crouch JE, Rosario-Ortiz FL, Jaffé R. 2017. Predicting reactive intermediate quantum yields from dissolved organic matter photolysis using optical properties and antioxidant capacity. Environ Sci Technol. 51(10):5404-5413.
5. Berg SM, Whiting QT, Herrli JA, Winkels R, Wammer KH, Remucal CK. 2019. The role of dissolved organic matter composition in determining photochemical reactivity at the molecular level. Environmental Science & Technology. 53(20):11725-11734.
6. Bricaud A, Morel A, Prieur L. 1981. Absorption by dissolved organic- matter of the sea (yellow substance) in the uv and visible domains. Limnology and Oceanography. 26(143-53).
7. Stedmon CA, Markager S, Kaas H. 2000. Optical properties and signatures of chromophoric dissolved organic matter (CDOM) in danish coastal waters. Estuarine Coastal and Shelf Science. 51(2):267-278.
8. Peuravuori J, Pihlaja K. 1997. Molecular size distribution and spectroscopic properties of aquatic humic substances. Anal Chim Acta. 337(2):133-149.
9. Duarte R, Santos EBH, Duarte AC. 2003. Spectroscopic characteristics of ultrafiltration fractions of fulvic and humic acids isolated from an eucalyptus bleached kraft pulp mill effluent. Water Research. 37(17):4073-4080.
10. Uyguner CS, Bekbolet M. 2005. Implementation of spectroscopic parameters for practical monitoring of natural organic matter. Desalination. 176(1-3):47-55.
11. Coble PG. 1996. Characterization of marine and terrestrial dom in seawater using excitation emission matrix spectroscopy. Marine Chemistry. 51(4):325-346.
12. Coble PG. 2007. Marine optical biogeochemistry: The chemistry of ocean color. Chemical Reviews. 107(2):402-418.
13. Shapiro J. 1957. Chemical and biologic studies on the yellow organic acids of lake water. Limnology and Oceanography. 2(3):161-179.
14. Green SA, Blough NV. 1994. Optical-absorption and fluorescence properties of chromophoric dissolved organic-matter in natural-waters. Limnology and Oceanography. 39(8):1903-1916.
15. Aiona PK, Luek JL, Timko SA, Powers LC, Gonsior M, Nizkorodov SA. 2018. Effect of photolysis on absorption and fluorescence spectra of light-absorbing secondary organic aerosols. ACS Earth and Space Chemistry. 2(3):235-245.
16. Xie HX, Aubry C, Zhang Y, Song GS. 2014. Chromophoric dissolved organic matter (CDOM) in first-year sea ice in the western canadian arctic. Marine Chemistry. 165:25-35.
17. Massicotte P, Markager S. 2016. Using a gaussian decomposition approach to model absorption spectra of chromophoric dissolved organic matter. Marine Chemistry. 180:24-32.
18. Ma JH, Del Vecchio R, Golanoski KS, Boyle ES, Blough NV. 2010. Optical properties of humic substances and CDOM: Effects of borohydride reduction. Environ Sci Technol. 44(14):5395-5402.

19. Golanoski KS, Fang S, Del Vecchio R, Blough NV. 2012. Investigating the mechanism of phenol photooxidation by humic substances. Environ Sci Technol. 46(7):3912-3920.
20. Sharpless CM. 2012. Lifetimes of triplet dissolved natural organic matter (DOM) and the effect of NaBH4 reduction on singlet oxygen quantum yields: Implications for DOM photophysics. Environ Sci Technol. 46(8):4466-4473.
21. Sharpless CM, Blough NV. 2014. The importance of charge-transfer interactions in determining chromophoric dissolved organic matter (CDOM) optical and photochemical properties. Environmental Science-Processes & Impacts. 16(4):654-671.
22. McKay G. 2020. Emerging investigator series: Critical review of photophysical models for the optical and photochemical properties of dissolved organic matter. Environmental Science-Processes & Impacts. 22(5):1139-1165.
23. Del Vecchio R, Blough NV. 2004. On the origin of the optical properties of humic substances. Environ Sci Technol. 38(14):3885-3891.
24. McKay G, Korak JA, Erickson PR, Latch DE, McNeill K, Rosario-Ortiz FL. 2018. The case against charge transfer interactions in dissolved organic matter photophysics. Environ Sci Technol. 52(2):406-414.
25. Blough NV, Del Vecchio R. 2018. Comment on the case against charge transfer interactions in dissolved organic matter photophysics. Environmental Science & Technology. 52(9):5512-5513.
26. McKay G, Korak JA, Erickson PR, Latch DE, McNeill K, Rosario-Ortiz FL. 2018. Response to comment on the case against charge transfer interactions in dissolved organic matter photophysics. Environmental Science & Technology. 52(9):5514-5516.
27. McKay G. 2021. Autoxidized hydroquinone mimics the optical properties of chromophoric dissolved organic matter. Environ. Sci. Technol. Lett. 8 (9): 825-831.
28. Vialykh EA, McKay G, Rosario-Ortiz FL. 2020. Computational assessment of the three-dimensional configuration of dissolved organic matter chromophores and influence on absorption spectra. Environmental Science & Technology. 54(24):15904-15913.
29. Casida ME. 1995. Time-dependent density functional response theory for molecules. In: Chong DP, editor. Recent advances in density functional methods, part 1. Singapore: World Scientific. p.155-192.
30. Furche F, Ahlrichs R, Wachsmann C, Weber E, Sobanski A, Vogtle F, Grimme S. 2000. Circular dichroism of helicenes investigated by time-dependent density functional theory. Journal of the American Chemical Society. 122(8):1717-1724.
31. Neese F. 2009. Prediction of molecular properties and molecular spectroscopy with density functional theory: From fundamental theory to exchange-coupling. Coordination Chemistry Reviews. 253(5-6):526-563.
32. Leenheer JA, McKnight DM, Thurman E, M., MacCarthy P. 1994. Structural Components and Proposed Structural Models of Fulvic Acid from the Suwannee River. In *Humic Substances in the Suwannee River, Georgia: Interactions, Properties, and Proposed Structures*, US Geological Servey, N.87-557; G.P.O., U. S., Eds. U.S. Geological Survey: 1994; pp 195–212.
33. Vialykh EA, Salahub DR, Achari G, Cook RL, Langford CH. 2019. Emergent functional behaviour of humic substances perceived as complex labile aggregates of small organic molecules and oligomers. Environmental Chemistry. 16(7):505-516.
34. Vialykh EA, Salahub DR, Achari G. 2020. Metal ion binding by humic substances as emergent functions of labile supramolecular assemblies. Environmental Chemistry. 17(3):252-265.

35. Pavlik JW, Perdue EM. 2015. Number-average molecular weights of natural organic matter, hydrophobic acids, and transphilic acids from the suwannee river, georgia, as determined using vapor pressure osmometry. Environmental Engineering Science. 32(1):23-30.
36. Appiani E, Page SE, McNeill K. 2014. On the use of hydroxyl radical kinetics to assess the number-average molecular weight of dissolved organic matter. Environ Sci Technol. 48 (20): 11794-11802
37. McAdams BC, Aiken GR, McKnight DM, Arnold WA, Chin YP. 2018. High pressure size exclusion chromatography (HPSEC) determination of dissolved organic matter molecular weight revisited: Accounting for changes in stationary phases, analytical standards, and isolation methods. Environmental Science & Technology. 52(2):722-730.
38. Remucal CK, Cory RM, Sander M, McNeill K. 2012. Low molecular weight components in an aquatic humic substance as characterized by membrane dialysis and orbitrap mass spectrometry. Environ Sci Technol. 46(17):9350-9359.
39. Maizel AC, Remucal CK. 2017. Molecular composition and photochemical reactivity of size-fractionated dissolved organic matter. Environmental Science & Technology. 51(4):2113-2123.
40. Neese F. 2012. The ORCA program system. Wiley Interdisciplinary Reviews-Computational Molecular Science. 2(1):73-78.
41. Plasser F, Wormit M, Dreuw A. 2014. New tools for the systematic analysis and visualization of electronic excitations. I. Formalism. Journal of Chemical Physics. 141(2).
42. Plasser F. 2020. TheoDORE: A toolbox for a detailed and automated analysis of electronic excited state computations. Journal of Chemical Physics. 152(8).
43. Hanwell MD, Curtis DE, Lonie DC, Vandermeersch T, Zurek E, Hutchison GR. 2012. Avogadro: An advanced semantic chemical editor, visualization, and analysis platform. Journal of Cheminformatics. 4.
44. Eaton JW, Bateman D, Hauberg S. 2009. GNU octave version 3.0.1 manual: A high-level interactive language for numerical computations. CreateSpace Independent Publishing Platform.
45. Leresche F, McKay G, Kurtz T, von Gunten U, Canonica S, Rosario-Ortiz FL. 2019. Effects of ozone on the photochemical and photophysical properties of dissolved organic matter. Environmental Science & Technology. 53(10):5622-5632.
46. Skoog DA, Holler FJ, Crouch SR. 2017. Principles of instrumental analysis. Cengage Learning.
47. Blank F. 1958. Anthocyanins, flavones, xanthones. In: Springer B, Heidelberg., editor. The metabolism of secondary plant products. p. 300-353.
48. Barcenas G, Biaggne A, Mass OA, Wilson CK, Obukhova OM, Kolosova OS, Tatarets AL, Terpetschnig E, Pensack RD, Lee J et al. 2021. First-principles studies of substituent effects on squaraine dyes. Rsc Advances. 11(31):19029-19040.
49. Hu ND, Gong YL, Wang XC, Lu Y, Peng GY, Yang L, Zhang ST, Luo ZP, Li HR, Gao F. 2015. A successful attempt to obtain the linear dependence between one-photon and two-photon spectral properties and hammett parameters of various aromatic substituents in new pi-extended asymmetric organic chromophores. Journal of Fluorescence. 25(6):1559-1566.
50. Meredith P, Sarna T. 2006. The physical and chemical properties of eumelanin. Pigment Cell Research. 19(6):572-594.

51. Pezzella A, Iadonisi A, Valerio S, Panzella L, Napolitano A, Adinolfi M, d'Ischia M. 2009. Disentangling eumelanin "Black chromophore": Visible absorption changes as signatures of oxidation state- and aggregation-dependent dynamic interactions in a model water-soluble 5,6-dihydroxyindole polymer. Journal of the American Chemical Society. 131(42):15270-15275.
52. Walrafen GE, Fisher MR, Hokmabadi MS, Yang WH. 1986. Temperature-dependence of the low-frequency and high-frequency raman-scattering from liquid water. Journal of Chemical Physics. 85(12):6970-6982.
53. Emamian S, Lu T, Kruse H, Emamian H. 2019. Exploring nature and predicting strength of hydrogen bonds: A correlation analysis between atoms-in-molecules descriptors, binding energies, and energy components of symmetry-adapted perturbation theory. Journal of Computational Chemistry. 40(32):2868-2881.
54. Grimme S. 2008. Do special noncovalent pi-pi stacking interactions really exist? Angewandte Chemie-International Edition. 47(18):3430-3434.
55. Liu ZY, Lu T, Chen QX. 2021. Intermolecular interaction characteristics of the all-carboatomic ring, cyclo 18 carbon: Focusing on molecular adsorption and stacking. Carbon. 171:514-523.
56. Liu B, Pang Y, Bouhenni R, Duah E, Paruchuri S, McDonald L. 2015. A step toward simplified detection of serum albumin on sds-page using an environment-sensitive flavone sensor. Chemical Communications. 51(55):11060-11063.
57. Liu B, McDonald L, Liu Q, Bi XM, Zheng J, Wang L, Pang Y. 2016. A flavonoid-based light-up bioprobe with intramolecular charge transfer characteristics for wash-free fluorescence imaging in vivo. Sensors and Actuators B-Chemical. 235:309-315.
58. Anh NV, Williams RM. 2012. Bis-semiquinone (bi-radical) formation by photoinduced proton coupled electron transfer in covalently linked catechol-quinone systems: Aviram's hemiquinones revisited. Photochemical & Photobiological Sciences. 11(6):957-961.
59. Staab HA, Herz CP. 1977. Diastereosiomeric 3.3 paracylophane quinhydrones. Angewandte Chemie-International Edition in English. 16(11):799-801.
60. Misra R, Chakraborty P, Roy SC, Maity DK, Bhattacharyya SP. 2016. Tailoring of spectral response and intramolecular charge transfer in beta-enaminones through band gap tuning: Synthesis, spectroscopy and quantum chemical studies. RSC Advances. 6(43):36811-36822.
61. Baluha DR, Blough NV, Del Vecchio R. 2013. Selective mass labeling for linking the optical properties of chromophoric dissolved organic matter to structure and composition via ultrahigh resolution electrospray ionization mass spectrometry. Environ Sci Technol. 47(17):9891-9897.
62. Andrew AA, Del Vecchio R, Subramaniam A, Blough NV. 2013. Chromophoric dissolved organic matter (CDOM) in the equatorial atlantic ocean: Optical properties and their relation to cdom structure and source. Marine Chemistry. 148:33-43.
63. Chen Y, Liu J, Zhang X, Blough NV. 2020. Time-resolved fluorescence spectra of untreated and sodium borohydride-reduced chromophoric dissolved organic matter. Environmental Science & Technology. 54(19):12109-12118.
64. Bianca MR, Baluha DR, Gonsior M, Schmitt-Kopplin P, Del Vecchio R, Blough NV. 2020. Contribution of ketone/aldehyde-containing compounds to the composition and optical properties of suwannee river fulvic acid revealed by ultrahigh resolution mass spectrometry and deuterium labeling. Analytical and Bioanalytical Chemistry. 412(6):1441-1451.

65. Schendorf TM, Del Vecchio R, Bianca M, Blough NV. 2019. Combined effects of pH and borohydride reduction on optical properties of humic substances (HS): A comparison of optical models. Environmental Science & Technology. 53(11):6310-6319.
66. Cartisano CM, Del Vecchio R, Bianca MR, Blough NV. 2018. Investigating the sources and structure of chromophoric dissolved organic matter (CDOM) in the north pacific ocean (NPO) utilizing optical spectroscopy combined with solid phase extraction and borohydride reduction. Marine Chemistry. 204:20-35.
67. Del Vecchio R, Schendorf TM, Blough NV. 2017. Contribution of quinones and ketones/aldehydes to the optical properties of humic substances (HS) and chromophoric dissolved organic matter (CDOM). Environmental Science & Technology. 51(23):13624-13632.
68. Guo RR, Ma JH. 2014. Reduction-induced molecular signature of humic substances: Structural evidence for optical changes. RSC Advances. 4(49):25880-25885.
69. Meingast KM, Grunert BK, Green SA, Kane ES, Khademimoshgenani N. 2020. Insights on dissolved organic matter production revealed by removal of charge-transfer interactions in senescent leaf leachates. Water. 12(9).
70. Osburn CL, Kinsey JD, Bianchi TS, Shields MR. 2019. Formation of planktonic chromophoric dissolved organic matter in the ocean. Marine Chemistry. 209:1-13.
71. Schendorf TM, Del Vecchio R, Koech K, Blough NV. 2016. A standard protocol for NaBH4 reduction of CDOM and HS. Limnology and Oceanography-Methods. 14(6):414-423.
72. Johnson MR, Rickborn B. 1970. Sodium borohydride reduction of conjugated aldehydes and ketones. Journal of Organic Chemistry. 35(4):1041-1045.
73. Brown MS, Rapoport H. 1963. The reduction of esters with sodium borohydride. Journal of Organic Chemistry. 28(11):3261-3263.
74. Pitchumani K, Velusamy P, Srinivasan C. 1994. Selectivity in sodium borohydride reduction of coumarin encapsulated in beta-cyclodextrin. Tetrahedron. 50(45):12979-12988.
75. Criswell TR, Klanderm.Bh. 1974. Studies related to the conversion of 9,10-anthraquinones to anthracenes. Journal of Organic Chemistry. 39(6):770-774.
76. Schauble JH, Walter GJ, Morin JG. 1974. Complex metal hydride reduction of carbon-carbon unsaturation. 1. Sodium-borohydride reduction of alpha-phenylcinnamates and related systems. Journal of Organic Chemistry. 39(6):755-760.
77. International Humic Substance Society (IHSS), ^{13}C NMR estimates of Carbon Distribution. https://humic-substances.org/13c-nmr-estimates-of-carbon-distribution-in-ihss-samples (accessed 03.IV.2018).